Lycopene-loaded hollow cerium oxide nanozymes restore mitochondrial dynamics, reprogram ROS/NAD+ redox, and suppress p53-p21 axis for treating senescence-driven osteoarthritis

Xueying An, Hanjie Zhang, Xujing Zhang, Minyi Cai, Yining Zhou, Hantao Cai, Tao Shen, Sheng zhao, Zhihong Xu, Hui Wei, Qing Jiang

PII: S1385-8947(26)08906-0

DOI: https://doi.org/10.1016/j.cej.2026.181443

Reference: CEJ 181443

To appear in:

Received date: 4 June 2026

Revised date: 5 August 2026

Accepted date: 31 August 2026

Please cite this article as: X. An, H. Zhang, X. Zhang, et al., Lycopene-loaded hollow cerium oxide nanozymes restore mitochondrial dynamics, reprogram ROS/NAD+ redox, and suppress p53-p21 axis for treating senescence-driven osteoarthritis, (2026), https://doi.org/10.1016/j.cej.2026.181443

Lycopene-Loaded Hollow Cerium Oxide Nanozymes Restore Mitochondrial Dynamics, Reprogram ROS/NAD^+ Redox, and Suppress p53-p21 Axis for Treating Senescence-Driven Osteoarthritis

Hollow CeO_2/Lycopene Nanozyme Remodels the Mitochondrial-Redox-Senescence Axis in OA

Xueying An[1, 3#], Hanjie Zhang[2#], Xujing Zhang[4#], Minyi Cai[1, 3], Yining Zhou[1, 3], Hantao Cai[1, 3], Tao Shen[1, 3], Sheng zhao[5], Zhihong Xu[1, 3, 7], Hui Wei[2, 6*], Qing Jiang[1, 3, 7*]*

1 Division of Sports Medicine and Adult Reconstructive Surgery, Department of Orthopedic Surgery, Nanjing Drum Tower Hospital, State Key Laboratory of Pharmaceutical Biotechnology, Nanjing University, Nanjing, Jiangsu, 210008, China.

2 Department of Biomedical Engineering, College of Engineering and Applied Sciences, Nanjing National Laboratory of Microstructures, Jiangsu Key Laboratory of Artificial Functional Materials, Nanjing University, Nanjing, Jiangsu, 210023, China.

3 Branch of National Clinical Research Center for Orthopedics, Sports Medicine and Rehabilitation, Nanjing, Jiangsu, 210008, China.

4 Department of Molecular and Cell Biology, College of Letters and Science, University of California, Berkeley, Berkeley, California, 94720, USA.

5 School of Chemistry and Chemical Engineering, Collaborative Innovation Center of Ecological Civilization, Hainan University, Haikou 570228, Hainan, China.

6 State Key Laboratory of Analytical Chemistry for Life Science, School of Chemistry and Chemical Engineering, Chemistry and Biomedicine Innovation Centre (ChemBIC),

ChemBioMed Interdisciplinary Research Centre at Nanjing University, Nanjing University, Nanjing, Jiangsu, 210023, China.

7 Co-innovation Center of Neuroregeneration , Nantong University, 19 Qixiu Road, Nantong 226001, PR China.

# These authors contributed equally to this work.

* Corresponding authors: xuzhihong@njglyy.com (Zhihong Xu), weihui@nju.edu.cn (Hui Wei), qingj@nju.edu.cn (Qing Jiang)

Abstract

Osteoarthritis (OA) is strongly associated with chondrocyte senescence, driven by oxidative stress, mitochondrial dysfunction, and the ensuing senescence-associated secretory phenotype (SASP). Herein, we report a lycopene-loaded ceria nanozyme (Ly@Ce) designed to simultaneously address these interconnected pathogenic cues. Ly@Ce markedly reduced intracellular and mitochondrial reactive oxygen species (ROS), mitigated excessive mitochondrial fragmentation, and restored mitochondrial membrane potential in senescent chondrocytes, indicating robust recovery of mitochondrial fitness. Notably, Ly@Ce also elevated intracellular nicotinamide adenine dinucleotide (NAD^+) levels, making it an active metabolic modulator rather than a passive ROS scavenger. Transcriptomic profiling revealed that Ly@Ce reversed H_2O_2-induced dysregulation of the p53-p21 signaling pathway, accompanied by suppression of SASP-related genes and a shift of extracellular matrix metabolism toward an anabolic program, thus delaying OA progression. Collectively, these findings establish Ly@Ce as a bioinspired, catalytic antioxidant nanoplatform that combines redox and NAD^+

reprogramming with p53-p21 inhibition, offering a disease-modifying strategy for senescence-associated OA and a potential framework for targeting other age-related pathologies characterized by mitochondrial decline and cellular senescence.

Keywords: Osteoarthritis; cellular senescence; nanozyme; mitochondrial dysfunction; metabolic reprogramming; p53-p21 axis; NAD^+.

1.1 Introduction

Osteoarthritis (OA) is a highly prevalent degenerative joint disease in the ageing population and a leading cause of chronic pain, functional disability, and reduced quality of life. [1 2] Age-related structural and biochemical changes in articular cartilage, synovium and subchondral bone, together with long-term mechanical overloading, lead to progressive cartilage erosion, osteophyte formation and joint space narrowing. [3 4] Increasing evidence indicates that oxidative stress and chronic low-grade inflammation are the main drivers of this pathogenesis. [5] Excessive generation of reactive oxygen species (ROS) disrupts redox homeostasis in chondrocytes and synoviocytes, accelerates extracellular matrix degradation, promotes cellular senescence and apoptosis, and amplifies pro-inflammatory signaling, ultimately aggravating structural damage in osteoarthritic joints. [6 7]

Current clinical management of OA primarily relies on oral analgesics (mainly non-steroidal anti-inflammatory drugs) and intra-articular injections (e.g., glucocorticoids and hyaluronic acid). [2 8 9] These approaches predominantly relieve symptoms but show limited capacity to inhibit or reverse disease progression and may cause considerable systemic side effects upon long-term administration. [10 11] Joint replacement surgery is effective for end-stage

disease but is invasive, costly and not suitable for all elderly patients. [12] Therefore, there is an urgent need for disease-modifying strategies that specifically modulate oxidative stress and inflammation in the joint microenvironment, particularly in age-related OA, which is characterized by pronounced redox imbalance and cellular aging.

Cerium oxide (CeO_2) nanozymes exploit reversible Ce^{3+}/Ce^{4+} redox cycling to mimic superoxide dismutase (SOD), and catalase (CAT), thereby scavenging a broad range of ROS and protecting tissues from oxidative injury. [13-16] When engineered as hollow nanospheres, CeO_2 provides a high surface area with abundant accessible active sites, while the internal cavity can be used to load therapeutic agents. [17 18] Such hollow CeO_2 nanozymes are therefore attractive platforms for joint-targeted antioxidant therapy, where sustained ROS elimination and local drug delivery are both required.

Lycopene is a natural carotenoid abundant in tomatoes and other red fruits, with potent antioxidant and anti-inflammatory activities. In joint-related models, lycopene alleviates oxidative stress, suppresses matrix metalloproteinase (MMP) expression, and modulates inflammatory cytokine secretion, supporting its chondroprotective potential. [19 20] Nevertheless, its application is limited by poor aqueous solubility, susceptibility to oxidative degradation and low bioavailability. [21 22] Encapsulating lycopene in nanocarriers has therefore been proposed to improve its stability in physiological environments, enhance bioavailability and enable sustained, targeted delivery to diseased joints.

In this work, hollow CeO_2 nanospheres were constructed and subsequently loaded with lycopene to obtain Ly@Ce, which provided a synergistic strategy for redox modulation in

osteoarthritic joints. The physicochemical characteristics, enzyme-like ROS-scavenging performance and general free-radical-quenching abilities of Ly@Ce were systematically evaluated, followed by investigation of its protective effects in aged chondrocytes and an OA model in elderly mice. We found that Ly@Ce nanozymes reprogrammed redox homeostasis in chondrocytes, leading to reduced ROS and elevated nicotinamide adenine dinucleotide (NAD^+) levels, which alleviated mitochondrial dysfunction and cellular senescence. Consistently, Ly@Ce inhibited the p53-p21 senescence axis and attenuated the secretion of senescence-associated secretory phenotype (SASP) factors (e.g., IGFBP5, IL13 and IL6). This suppression remodeled chondrocyte extracellular matrix metabolism by downregulating matrix catabolic genes and elevating anabolic markers, thus delaying OA progression. This study establishes Ly@Ce as a versatile antioxidant nanoplatform and provides proof-of-concept evidence for nanozyme-based redox modulation as a disease-modifying strategy for OA.

1.2 Experimental and Methods

1.2.1 Chemicals and reagents

Polyvinylpyrrolidone K30 (PVP-K30), potassium persulfate ($K_2S_2O_8$) and nitrotetrazolium blue chloride (NBT) were purchased from Aladdin Chemical Co., Ltd. (Shanghai, China). Cerium nitrate hexahydrate ($Ce(NO_3)_3 \cdot 6H_2O$) and riboflavin were purchased from J&K Scientific Co., Ltd. Ethylene glycol (EG), hydrochloric acid (HCl), hydrogen peroxide (H_2O_2) and disodium edetate dihydrate (EDTA-2Na) were purchased from Sinopharm Chemical Reagent Co., Ltd. (Shanghai, China). Lycopene were purchased from Beijing Solarbio Science & Technology Co., Ltd. ABTS (2,2'-azino-bis(3-ethylbenzothiazoline-6-sulfonic acid) was purchased from Macklin

Biochemical Co., Ltd. (Shanghai, China). DPPH (1,1-diphenyl-2-picryl-hydrazyl) was obtained from Yuanye Biotechnology Co., Ltd. (Shanghai, China). 5,5-Dimethyl-1-pyrroline N-oxide (DMPO) and Cell Counting Kit-8 (CCK-8) were purchased from MedChemExpress (New Jersey, USA). 2',7'-Dichlorodihydrofluorescein diacetate (DCFH-DA) was purchased from AbMole (Houston, USA). All chemicals were purchased from commercial sources and used directly without further purification. Ultrapure water (18 MΩ•cm) was obtained from a Milli-Q purification system.

1.2.2 Instrumentations

Powder X-ray diffraction (XRD) data were recorded with 5 °/min on a D8 advance X-ray diffractometer (Bruker-AXS, Germany). Dynamic light scattering (DLS) and zeta potential results were recorded by using a Zetasizer NanoZSP (Malvern, UK). X-ray photoelectron spectroscopy (XPS) spectra were collected by using a PHI 5000 Versa Probe XPS microscope (Ulvac-Phi, Japan). Transmission electron microscopy (TEM) images was obtained from a JEM-1400Flash (JEOL, Japan). Inductively coupled plasma (ICP) was performed by using a ICAP7400 ICP-OES instrument (Thermo Fisher Scientific, USA). Electron paramagnetic resonance (EPR) spectra were recorded on a A300 spectrometer (Bruker, USA). Ultraviolet-visible absorption spectra were measured by using a SpectraMax M2e microplate reader (Molecular Devices, USA) or a UV-3600 Plus UV-vis spectrophotometer (Shimadzu, Japan). Dissolved oxygen experiment was performed by using InLab OptiOx detector (Mettler Toledo, Switzerland).

1.2.3 Synthesis of hollow CeO_2 and Ly@Ce

hollow CeO_2 nanospheres were synthesized following a previously reported procedure with slight modifications. [23] Typically, 1.0 g of $Ce(NO_3)_3 \cdot 6H_2O$ and 0.4 g of PVP-K30 were dissolved in 30 mL of EG and stirred for 30 min. After that, 1 mL of 1.0 M aqueous HCl was added under vigorous stirring. The resulting clear solution was stirred for a further 30 min and then transferred into a 50 mL Teflon-lined stainless-steel autoclave, which was heated at 165 °C for 3 h. After naturally cooling to room temperature, the gray product was collected by centrifugation, washed several times with deionized water (10000 rpm, 20 min), and finally dried at 60 °C overnight for subsequent characterization.

Ly@Ce was prepared as follows. A freshly synthesized aqueous dispersion of CeO_2 (7.5 mL, 1 mg/mL) was added to an ethyl alcohol solution of lycopene (15 mL, 0.5 mg/mL) under magnetic stirring, and the mixture was allowed to react for 24 h at room temperature. The resulting suspension was centrifuged to collect the precipitate, which was washed three times with deionized water to afford the Ly@Ce nanocomposite. Cy3@Ce was synthesized following the same procedure described above for cell uptake and *in vivo* imaging.

1.2.4 Measurement of CAT-like activity

The CAT-like activity of CeO_2 and Ly@Ce was determined using a dopamine-based universal assay as previously described. [24] Briefly, reactions were performed in a 96-well plate with a total volume of 200 μL, containing 5 μL of nanozyme dispersion (12.5, 25, or 50 μg/mL), 90 μL of Tris buffer (10 mM, pH 8.5), 100 μL of dopamine solution (2 mg/mL), and 5 μL of H_2O_2 (0.8 M). Immediately after mixing, the plate was transferred to an anaerobic chamber and incubated at 37 °C for 25 min, after which the absorbance at 405 nm was recorded using a microplate reader.

1.2.5 Measurement of SOD-like activity

The SOD-like activity of CeO_2 and Ly@Ce was evaluated by monitoring the scavenging of $O_2^{\bullet-}$ using NBT as the probe. Briefly, NBT (60 μM), EDTA-2Na (8 mM), riboflavin (24 μM) and the nanozyme at different concentrations (12.5, 25, or 50 μg/mL) were mixed in PBS (0.1 M, pH 7.4) and incubated in the dark for 5 min. The mixtures were then irradiated with a 27 W light source for 150 s, and the absorbance at 580 nm was recorded using a microplate reader. The elimination ratio of $O_2^{\bullet-}$ was calculated as (1- A/A_0), where A and A_0 are the absorbances at 580 nm in the presence and absence of the nanozyme, respectively.

1.2.6 Measurement of $^{\bullet}OH$ scavenging activity

$^{\bullet}OH$ were generated via the Fenton reaction by mixing Fe^{2+} (0.5 mM) with H_2O_2 (0.5 mM) in PBS (0.1 M, pH 7.4). The trapping agent DMPO (10 mM) and the nanozyme (100 μg/mL) were then added to the reaction mixture. After incubation for 90 s, the solution was drawn into a quartz capillary, placed in a glass EPR tube, and subjected to EPR analysis.

1.2.7 Measurement of DPPH$^{\bullet}$ scavenging activity

The DPPH$^{\bullet}$ scavenging activity of the CeO_2 and Ly@Ce was determined by monitoring the change in absorbance at 520 nm. In a typical experiment, the nanozyme was added to a methanolic DPPH solution (5 μg/mL), and the mixture was vortexed thoroughly and incubated at 37 °C in the dark for 1 h. The absorbance at 520 nm was subsequently measured using a microplate reader. The radical scavenging ratio was calculated in the same manner as that used for the SOD-like activity assay.

1.2.8 Measurement of ABTS$^{\bullet+}$ scavenging activity

The $ABTS^{\bullet+}$ scavenging activity of the CeO_2 and Ly@Ce was determined by monitoring the decrease in absorbance at 734 nm. Briefly, $ABTS^{\bullet+}$ solution was prepared by mixing aqueous K $K_2S_2O_8$ (2.45 mM, 10 mL) and ABTS (7 mM, 10 mL), incubating the mixture in the dark for 12 h. The resulting $ABTS^{\bullet+}$ solution was then diluted tenfold. Nanozyme samples were added to the diluted $ABTS^{\bullet+}$ solution and incubated at 37 °C for 1 h, after which the absorbance at 734 nm was recorded using a microplate reader. The radical scavenging ratio was calculated in the same manner as for the SOD-like activity assay.

1.2.9 Cell uptake

Chondrocytes were cultured in confocal dishes overnight and then exposed to Cy3@Ce (10 μg/mL CeO_2) for 3 h or 6 h at 37 °C. After washed by PBS, the cells were stained with LysoPrime Green (Dojindo Laboratories, Japan) and Hoechst to label lysosomes and nuclei. The intracellular distribution of Cy3@Ce (red) and its colocalization with lysosomes (green) were examined under a confocal microscope (LSM900, Germany).

1.2.10 Cell viability assay

Cell viability was assessed by Cell Counting Kit-8 (CCK8; MedChemExpress, Shanghai, China) according to the manufacturer's instructions. Briefly, C28/I2 cells were seeded in 96-well plates and cultured overnight. For toxicity detection of nanoparticles, C28/I2 cells were treated with different concentrations of CeO_2 (CeO_2, 5 μg/mL and 10 μg/mL), and Ly@Ce (CeO_2, 5 μg/mL and 10 μg /mL). For the effects of H_2O_2 and nanoparticles, four treatment groups were used: Ctrl (untreated), H_2O_2 (400 μM), CeO_2 (10 μg/mL) and Ly@Ce (CeO_2, μg/mL) under H_2O_2 treatment. Following above treatments, 10 μL of CCK-8 reagent was added to each well and the plates were

incubated at 37 °C for 2 hours. The absorbance at 450 nm was measured by a microplate reader (Molecular Devices M3, USA). The viability of treated cells was normalized by Ctrl group.

1.2.11 Senescence detection assay

Cellular senescence was evaluated using a β-Galactosidase Staining Kit (Beyotime, Shanghai, China). Cells were seeded in 6-well plates and administrated with Ctrl (untreated), H_2O_2 (400 μM), CeO_2 (10 μg/mL) and Ly@Ce (CeO_2, 10 μg/mL) under H_2O_2 treatment. Chondrocytes in 6-well plates were treated with H_2O_2 (400 μM) alone or in combination with Lycopene (10 μg/mL), CeO_2 (10 μg/mL), Lycopene + CeO_2 (each 10 μg/mL), or Ly@Ce (10 μg/mL CeO_2-equiv.) to evaluate their synergistic protective effects. After washing with PBS, cells were fixed with the provided fixation solution for 15 minutes at room temperature. Subsequently, cells were incubated with the β-galactosidase staining working solution (containing X-Gal) at 37 °C overnight in a dry incubator. Senescent cells were observed and imaged by a bright-field microscope (Nikon, Japan).

1.2.12 Total ROS detection assay

Intracellular reactive oxygen species (ROS) were measured using the fluorescent probe 2',7'-dichlorodihydrofluorescein diacetate (DCFH-DA; AbMole, USA). After treatment, C28/I2 cells were washed with serum-free medium and incubated with 10 μM DCFH-DA at 37 °C for 30 minutes in the dark. Then washed twice with PBS and fluorescent images were captured using a fluorescence microscope (Leica, Wetzlar, Germany).

1.2.13 Determination of NAD^+/NADH levels

Intracellular NAD^+/NADH levels were detected by NAD^+/NADH Detection Kit purchased from

Beyotime (Shanghai, China). C28/I2 cells were lysed by NAD^+/NADH extraction buffer. The lysate was centrifuged at 12,000×g for 5-10 minutes at 4 ℃. The supernatant was collected as the test sample. Some samples was heated at 60 ℃ in a water bath or PCR machine for 30 minutes to degrade NAD^+. Ethanol dehydrogenase working solution was then added and thoroughly mixed. The mixture was incubated at 37 ℃ in the dark for 10 min. then read the absorbance at 450 nm using a microplate reader (Nikon, Tokyo, Japan).

1.2.14 Mitochondrial morphology analysis

Mitochondrial morphology was identified by MitoTracker® Green FM (CST, Danvers, USA). Cells were seeded in 12-well plates and administrated with Ctrl (untreated), H_2O_2 (400 μM), CeO_2 (10 μg/mL) and Ly@Ce (CeO_2, 10 μg/mL) under H_2O_2 treatment. Then C28/I2 cells were were incubated with 100 nM mitochondrial staining solution and Hoechst 33342 nuclear staining reagent (Beyotime, Shanghai, China) for 30 minutes at 37℃. Then, they were washed three times with HBSS and immediately photographed by confocal (LSM900, ZEISS, Germany).

1.2.15 Assessment of mitochondrial function

Mitochondrial membrane potential was assessed using JC-1 (MCE, shanghai, China), and mitochondrial ROS detection was performed using mitoSOX Red (Thermo Fisher Scientific, Shanghai, China). Briefly, C28/I2 cells were treated with Ctrl (untreated), H_2O_2 (400 μM), CeO_2 (10 μg/mL) and Ly@Ce (CeO_2, 10 μg/mL) under H_2O_2 treatment. Cells were stained with two dyes using working-concentration staining solutions specified in the manual, and images were captured by fluorescence microscopy (Leica, Wetzlar, Germany).

1.2.16 Animal study

The 6-month and 18-month C57BL/6 mice were purchased from the Model Animal Research Center of Nanjing University. All animal feeding and experimental procedures were approved by the Ethics Committee and the Institutional Animal Care and Use Committee of Drum Tower Hospital, Nanjing University Medical School. The animal studies involved 4 groups: 6-month-old (Young), 18-month-old (Old), 18-month-old + CeO_2 (Old + CeO_2, 5 mg/kg, once weekly, intra-articular injection), and 18-month-old + Ly@Ce (Old + Ly@Ce, at a CeO_2-equivalent dose of 5 mg/kg once weekly). After 9 weeks treatment, all mice were sacrificed by isoflurane overdose, and Knee Joints, heart, liver, spleen, lung and kidney were collected. 8-week-old male mice were treated with Lycopene (5 mg/kg), CeO_2 (5 mg/kg), and Ly@Ce (5 mg/kg CeO_2-equiv.) for 1 week, after which H&E staining of major organs (heart, liver, spleen, lungs, kidneys) was performed.

For *in vivo* imaging. 8-week-old mice were intra-articular injected by Cy3@Ce (5 mg/kg CeO_2-equiv.). Fluorescence images were captured at day 1, day 3, and day 7 post-injection under anesthesia using an in vivo imaging system (AniView, China).

1.2.17 Micro-Computed Tomography (Micro-CT)

After the knee joints of the mice were collected, they were fixed with 4% paraformaldehyde for more than 24 hours, and then scanned by micro-CT (vivaCT80, SCANCO Medical AG, Switzerland). Subsequently, 3D reconstruction was performed on all the joint bones by CT analysis software.

1.2.18 Immunostaining analyses (Safranin O-Fast Green Staining, IHC, and Immunofluorescence)

For cell immunofluorescence, C28/I2 cells were fixed by 4% paraformaldehyde, and Triton X-100 treatment, and goat serum for blocking. Then incubated overnight at 4 °C with primary antibodies (anti-p21, Cat No. 10355-1-AP, anti-MMP3, Proteintech, Cat No. 17873-1-AP; anti-COL2, Boster, BA0533; anti-p-p53, Proteintech, Cat No. 28961-1-AP; anti-SIRT1, Cell signaling technology, Cat No. 8469S). Then incubated with Alexa Fluor-conjugated secondary antibodies (Thermo Fisher Scientific, Shanghai, China) and counterstained with DAPI. Images were acquired by a fluorescence microscope (Leica, Wetzlar, Germany). Immunofluorescence was analyzed using Fiji software.

For tissue histological evaluation, knee joints of the mice were collected and fixed, then decalcified, paraffin-embedded and sectioned at 5 μm thickness. Safranin O-Fast Green Staining was performed following standard protocols. For immunohistochemistry (IHC) and immunofluorescence (IF), antigen retrieval was performed using antigen recovery solution (Beyotime, Shanghai, China). Sections were blocked with 5% normal goat serum and incubated overnight at 4 °C with primary antibodies (anti-p-p53, Proteintech, Cat No. 28961-1-AP; anti-IL6, Proteintech, Cat No. 66146-1-Ig; anti-p21, Proteintech, Cat No. 10355-1-AP, anti-ADAMTS5, CST, 14351; anti-COL2, Boster, BA0533). For IHC, detection was carried out using a horseradish peroxidase (HRP)-conjugated secondary antibody and 3,3'-diaminobenzidine (DAB) chromogen. For IF, sections were incubated with Alexa Fluor-conjugated secondary antibodies (Thermo Fisher Scientific, Shanghai, China) and counterstained with DAPI. Images were acquired using a light microscope (VS200, Olympus, Japan) or a fluorescence microscope (Leica, Wetzlar, Germany). Immunofluorescence was analyzed using Fiji software.

1.2.19 Transcriptome sequencing and analyses

The transcriptome sequencing was performed using the Illumina Novaseq 6000 sequencing platform, and the library construction was carried out using the Illumina TruseqTM RNA sample preparation kit method. Differential expression analysis was performed with the DESeq2 R package. Genes with p-value < 0.05 and |Fold change| > 1.5 were considered differentially expressed. Gene Ontology (GO), Gene Set Enrichment Analysis (GSEA) and Kyoto Encyclopedia of Genes and Genomes (KEGG) pathway enrichment analyses were conducted using clusterProfiler. Differential gene heatmap analysis was conducted by Hiplot tool. Transcriptome sequencing and analysis were performed by Hangzhou Cosmos Wisdom Biotech Co., Ltd.

1.2.20 Statistical analysis

Statistical analyses were performed using Prism 7 (GraphPad Software, Inc.). Data was presented as mean ± SD. Statistical differences were analyzed by one-way ANOVA and Student's t-test: *p<0.05, **p<0.01, ,and ***p<0.001.

1.3 Results

1.3.1 Preparation and characterization of lycopene-loaded hollow CeO_2 nanozymes

Hollow CeO_2 nanospheres were first obtained *via* a one-pot solvothermal reaction of cerium nitrate and PVP-K30 in ethylene glycol in the presence of HCl, and lycopene was subsequently introduced by incubating the hollow CeO_2 with a lycopene solution in ethyl alcohol (Figure 1A). This simple two-step procedure yielded lycopene-loaded hollow CeO_2 nanozymes, denoted as Ly@Ce.

The crystalline structures of CeO_2 and Ly@Ce were characterized by X-ray diffraction (XRD). Both samples displayed diffraction peaks that can be indexed to the fluorite-type CeO_2 phase (PDF#43-1002) without any additional reflections (Figure 1B), indicating that the loading of lycopene did not alter the crystalline framework of ceria. Transmission electron microscopy (TEM) images revealed that the as-prepared CeO_2 consisted of uniform hollow nanospheres with an average particle size of 95.13 ± 0.97 nm (Figures 1C and S1A). After loading Ly@Ce retained the well-defined hollow morphology and shell structure, with a comparable average size of 95.51 ± 0.80 nm and a similarly narrow size distribution (Figures 1D and S1B), confirming that the encapsulation process did not collapse the nanocavities. Dynamic light scattering (DLS) analysis showed that the hydrodynamic diameter increased slightly from 151.6 ± 1.1 nm for CeO_2 to 162.8 ± 0.3 nm for Ly@Ce after lycopene loading (Figure 1E). Both samples exhibited narrow and unimodal particle-size distributions, indicating that lycopene incorporation did not obvious aggregation and that Ly@Ce retained good colloidal dispersity.. In addition, the zeta potential of the hollow CeO_2 nanospheres was markedly reduced after lycopene incorporation (from ~18.6 mV to ~5.6 mV, Figure S2). Ultraviolet-visible spectroscopy (UV-vis) provided further evidence for successful lycopene loading. Compared with bare CeO_2, Ly@Ce exhibited enhanced absorbance in the visible region (Figure S3A). Using the lycopene calibration curve at 475 nm (Figure S3B), the lycopene loading of Ly@Ce was determined to be 50 wt% by quantifying the residual lycopene in the supernatant. Furthermore, Fourier-transform infrared spectroscopy (FTIR) analysis was performed to confirm the successful incorporation of lycopene into hollow CeO_2 (Figure S4). Compared with pristine lycopene and CeO_2, Ly@Ce exhibited

characteristic vibrations from both components, including the C=C/C–H stretching bands of lycopene and Ce–O vibration of CeO_2, demonstrating the successful formation of the Ly@Ce. Then, the *in vitro* release behavior of lycopene form hollow CeO_2 was investigated in PBS. As shown in Figure 1F, Ly@Ce exhibited sustained lycopene release over 96 h under all tested conditions without an obvious initial burst. Under physiological conditions (pH 7.4), the cumulative release reached 77.0% at 96 h. Mildly acidic conditions (pH 6.5) moderately accelerated lycopene release, increasing the cumulative release to 83.1%, while the presence of H_2O_2 under mildly acidic conditions further increased the apparent cumulative release to 88.2%. These results indicated that Ly@Ce maintained a sustained-release profile under physiological conditions, whereas the mildly acidic and oxidative microenvironment facilitated lycopene release. This release behavior may improve the local availability of lycopene and support prolonged therapeutic effects in osteoarthritic joints.

The surface valence state of cerium was further analyzed by high-resolution Ce 3*d* X-ray photoelectron spectroscopy (XPS). Deconvolution of the Ce 3*d* spectra demonstrated the coexistence of Ce^{3+} and Ce^{4+} species in both samples (Figure 1G and H). The Ce^{3+} fraction was calculated to be 46.66 % for hollow CeO_2 and 45.71 % for Ly@Ce. Lycopene loading slightly increased the abundance of oxygen-vacancy-associated Ce^{3+} sites. Importantly, the mixed-valence character was preserved, supporting the enzyme-like activity.

These data confirmed that lycopene had been efficiently encapsulated within the hollow CeO_2 nanospheres while maintaining their structural integrity and redox-active surface, thereby establishing Ly@Ce as a promising antioxidant nanozyme platform for subsequent biological

studies.

1.3.2 Enzyme-like activities assay of CeO_2 and Ly@Ce

To assess the antioxidant nanozyme performance, the multi-enzyme-like activities of hollow CeO_2 and Ly@Ce were systematically evaluated (Figures 1I-L and S5). In the dopamine-based CAT assay, both materials showed pronounced, concentration-dependent decomposition of H_2O_2 (Figure 1I). The absorbance at 405 nm changed only slightly upon lycopene loading, indicating that Ly@Ce retained the intrinsic CAT-like activity of hollow CeO_2. The SOD-like activity was examined using the NBT reduction system. As the nanozyme concentration increased from 12.5 to 50 μg/mL, the $O_2^{\bullet-}$ elimination efficiency of both samples rose steeply, reaching almost complete scavenging at the highest dose (Figure 1J). Notably, Ly@Ce consistently exhibited a slightly higher $O_2^{\bullet-}$ removal ratio than bare CeO_2, suggesting that lycopene incorporation did not hinder and may even facilitated superoxide scavenging. Hydroxyl radical ($^{\bullet}OH$) quenching was further probed by electron paramagnetic resonance (EPR) spectroscopy. The characteristic four-line spectrum (1:2:2:1) of DMPO-$^{\bullet}OH$ observed in the control group was markedly attenuated in the presence of CeO_2 or Ly@Ce (Figure 1K). In addition to enzyme-mimetic ROS removal, $DPPH^{\bullet}$ and $ABTS^{\bullet+}$ assays were employed to evaluate the general free radical scavenging capacity. Ly@Ce displayed significantly higher $DPPH^{\bullet}$ scavenging ratios than CeO_2 at all tested concentrations, reaching ~70 % elimination at 100 μg/mL (Figure 1L). A similar trend was observed for $ABTS^{\bullet+}$, where Ly@Ce afforded comparable activity at low concentration and a clearly superior scavenging performance at medium and high concentrations (Figure S5). Collectively, these results demonstrated that Ly@Ce inherited the multi-enzyme-like ROS

scavenging properties of hollow CeO_2 while benefiting from the additional radical-quenching contribution of lycopene, thereby providing a broad-spectrum antioxidant nanozyme platform.

Then, XPS was further performed to investigate the Ce valence state evolution during the enzyme-like catalytic process. Considering that the generation and regulation of $O_2^{\bullet-}$ during the SOD-like reaction are relatively complex, the CAT-like reaction with H_2O_2 was selected as a more controllable model to investigate the Ce^{3+}/Ce^{4+} redox evolution during catalytic turnover. The initial Ce^{3+} fractions of CeO_2 and Ly@Ce were comparable (46.66% and 45.71%, respectively, Figure 1G and H). After the CAT-like catalytic reaction with H_2O_2, the Ce^{3+} fraction decreased to 37.24% for CeO_2, whereas Ly@Ce retained a higher Ce^{3+} proportion (39.24%), suggesting that lycopene could facilitate the maintenance of Ce^{3+}/Ce^{4+} redox equilibrium during catalytic turnover (Figure S6).

Furthermore, H&E staining of major organs (heart, liver, spleen, lungs, and kidneys) revealed no obvious histological abnormalities after treated with Ly@Ce, confirming the favorable in vivo biocompatibility of Ly@Ce (Figure S7). Cellular uptake assays showed that Cy3@Ce was efficiently internalized by chondrocytes and no significant colocalization was observed between Cy3@Ce and lysosomes, indicating successful lysosomal escape (Figure S8). Furthermore, in vivo fluorescence imaging following intra-articular injection of Cy3@Ce demonstrated strong joint retention at day 1 and day 3, and only trace residual signal at day 7 (Figure S9).

1.3.3 Ly@Ce nanozyme attenuates chondrocyte senescence and cellular oxidative stress levels

We first evaluated the cytotoxicity of CeO_2 and Ly@Ce on chondrocytes by using Cell Counting

Kit-8 (CCK-8). Neither CeO_2 nor Ly@Ce caused detectable cytotoxicity at concentrations up to 10 μg/mL after 24 or 48 h incubation (Figure 2A). Chondrocyte senescence was then induced by H_2O_2, which markedly decreased cell viability. Treatment with CeO_2 or Ly@Ce significantly rescued cell viability, with Ly@Ce showing a more pronounced protective effect (Figure 2B). Given the central role of NAD^+ in cellular senescence, [25] we measured intracellular NAD^+ levels using NAD^+/NADH probes. H_2O_2 exposure led to a substantial reduction in the NAD^+/NADH ratio, whereas nanozyme administration restored NAD^+ redox balance, again with Ly@Ce outperforming CeO_2 (Figure 2C). Senescence-associated β-galactosidase (SA-β-gal) staining revealed a pronounced decrease in positively stained cells after CeO_2 or Ly@Ce treatment (Figure 2D and S10). Consistently, DCFH-DA staining revealed that Ly@Ce markedly decreased intracellular ROS accumulation compared with H_2O_2 and CeO_2 groups, indicating enhanced ROS-scavenging efficiency in senescent chondrocytes (Figure 2E and S11). As elevated p21 expression is a well-established marker of senescence, [26] we also examined p21 expression after nanozymes treatment. Compared with the H_2O_2 group, the Ly@Ce group showed a significant reduction in p21-positive cells (Figure 2F and S12). Together, these results demonstrated that Ly@Ce nanozyme could effectively restore redox homeostasis, alleviate oxidative stress and suppress senescence phenotypes in chondrocytes.

1.3.4 Ly@Ce nanozyme alleviates OA progression in aged mice

Ageing is a major risk factor for cartilage degeneration and the development of OA. [27 28] To evaluate the therapeutic potential of Ly@Ce in age-related OA, we employed 18-month-old naturally aged mice. After treatment with the two different nanozymes for 9 weeks, micro-CT

analysis showed that prominent osteophyte formation in aged joints compared with young controls (6-month-old), whereas nanozymes treatment attenuated osteophyte development, with Ly@Ce producing a more evident reduction than CeO_2 (Figures 3A and B). Histological evaluation by Safranin O-Fast Green staining showed marked loss of proteoglycan staining and thinning of the articular cartilage in aged mice. Notably, Ly@Ce substantially preserved cartilage architecture and increased the thickness of the uncalcified cartilage layer relative to the old group and the CeO_2 group (Figures 3C and D). Immunohistochemical staining of cartilage extracellular matrix metabolism further demonstrated that Ly@Ce downregulated the catabolic marker ADAM Metallopeptidase with Thrombospondin Type 1 Motif 5 (ADAMTS5) and upregulated the anabolic marker type II collagen (COL2) (Figure 3E, F and S13), indicating a shift in extracellular matrix metabolism toward a protective and pro-anabolic state in aged mice. Overall, these results supported that Ly@Ce nanozymes effectively mitigated age-related osteoarthritic degeneration and preserved cartilage integrity.

1.3.5 Ly@Ce nanozyme remodels chondrocyte extracellular matrix metabolism and alleviates mitochondrial damage

Encouraged by the protective effects of Ly@Ce in naturally aged mice, we next performed *in vitro* studies to explain the cellular basis of these improvements. Specifically, we examined whether Ly@Ce preserved chondrocyte matrix homeostasis and mitochondrial fitness during aging. As shown in Figure 4A-D and S14, Ly@Ce nanozyme treatment increased the expression of COL2 and decreased matrix metalloproteinase-3 (MMP3) compared with the H_2O_2-only and CeO_2-treated groups, indicating that Ly@Ce effectively improved extracellular matrix

homeostasis and attenuated senescence-associated OA-like changes. Given the relationship between mitochondrial dysfunction and cellular aging, [29] we next evaluated mitochondrial morphology and integrity in chondrocytes. Translocase of Outer Mitochondrial Membrane 20 (Tomm20) staining revealed severe mitochondrial fragmentation and network disruption in H_2O_2-treated chondrocytes, which were partially alleviated by CeO_2 and further restored by Ly@Ce (Figure 4E). Consistent with this, MitoSOX Red staining revealed pronounced mitochondrial ROS accumulation in H_2O_2-induced senescent chondrocytes, which was markedly reduced by Ly@Ce compared with CeO_2 (Figure 4F and S15A). Furthermore, mitochondrial membrane potential, a key indicator of functional fitness, was assessed by using a JC-1 probe. H_2O_2 treatment increased JC-1 monomer fluorescence and decreased aggregate fluorescence, reflecting a mitochondrial membrane potential loss. In contrast, Ly@Ce treatment restored the mitochondrial membrane potential more effectively than CeO_2 (Figure 4G and S15B). Together, these data demonstrated that Ly@Ce not only mitigated OA-related phenotypic changes in chondrocytes but also alleviated mitochondrial dysfunction in senescent cells.

1.3.6 Ly@Ce suppresses chondrocyte senescence by inhibiting p53-p21 axis

To elucidate how Ly@Ce regulated chondrocyte function, we performed transcriptome sequencing. Compared with the control group, H_2O_2-induced senescence resulted in 3,008 upregulated and 1,467 downregulated differentially expressed genes (DEGs) (Figure 5A and B). In contrast, Ly@Ce treatment led to the upregulation of 1,563 genes and the downregulation of 3,471 genes (Figure 5C and D). Kyoto Encyclopedia of Genes and Genomes (KEGG) pathway analysis of DEGs after H_2O_2 exposure and Ly@Ce administration revealed significant regulation

of both the cell cycle and p53 signaling axes across different groups (Figure 5E and F). Gene Set Enrichment Analysis (GSEA) demonstrated significant upregulation of Cell senescence axis DEGs in H_2O_2-treated chondrocytes, an effect that was robustly reversed by Ly@Ce treatment (Figure 5G and H), which also confirmed anti-aging effect of Ly@Ce. Collectively, these transcriptomic findings indicated that Ly@Ce mediated suppression of chondrocyte senescence may involve the p53-p21 axis.

Active phosphorylated p53 (p-p53) primarily influences cell cycle progression through the downstream regulatory mediator p21, causing cellular senescence and SASP production. [30] We next examined transcriptional changes in genes associated with the p53-p21 pathway. H_2O_2 treatment triggered marked upregulation of TP53I3 and CDKN1A (which encodes p21), indicative of robust p53 pathway activation. Concurrently, key cell-cycle regulators (CDK2, CDK6, CCNB1) were downregulated. Heatmap analysis further revealed concomitant alterations in chondrocyte extracellular-matrix metabolism and SASP factors: expression of the anabolic marker ACAN decreased, while catabolic markers (ADAMTS4, MMP25) and SASP-related genes (IL13, IGFBP5) were increased (Figure 6A and B). Importantly, treatment with Ly@Ce reversed these changes, normalizing the expression of p53-p21 pathway components, matrix-metabolism indicators, and SASP factors (Figure 6C and D). qPCR analysis further revealed that Ly@Ce treatment significantly upregulated the expression of the p21 gene (CDKN1A), while downregulating the mRNA levels of CDK2, CDK6, and CCNB1 (Figure S16). Together, these data demonstrated that Ly@Ce effectively counteracted H_2O_2-induced p53-p21 pathway activation, metabolic imbalance, and SASP production in chondrocytes. Consistent with

our *in vitro* observations, immunofluorescence analysis of aged mouse cartilage revealed increased expression of p-p53, p21, and IL-6. Treatment with CeO_2 or Ly@Ce significantly reduced the levels of all three proteins, with the effect being more pronounced in the Ly@Ce group (Figures 6E-G, S17 and S18). Since SIRT1 mediates NAD^+-dependent p53 activation, we assessed its expression following Ly@Ce treatment. Immunofluorescence analysis showed that Ly@Ce markedly upregulated the SIRT1 expression and reduced the number of p53-positive cells (Figures S19), indicating suppression of the p53 axis.

Synergistic experiments further confirmed the superiority of Ly@Ce over free lycopene, CeO_2 alone, or their physical mixture. Ly@Ce treatment led to the lowest SA-β-gal-positive cell rate and ROS levels among all groups (Figures S20). Moreover, compared with the Lyco + CeO_2 mixture, Ly@Ce more effectively upregulated SIRT1 expression and reduced p53-positive cells (Figures S21), suggesting that nanoencapsulation of lycopene with CeO_2 synergistically enhances anti-senescence efficacy via the SIRT1/p53 pathway. These results confirmed that Ly@Ce mitigated the SASP and extracellular matrix dysregulation in chondrocytes through inhibiting p53-p21 axis, thereby attenuating cellular senescence and OA progression.

1.4 Discussion and Conclusion

The development of effective therapeutics for senescence-associated OA necessitates interventions that can simultaneously target the fundamental drivers of chondrocyte aging: oxidative stress, mitochondrial dysfunction, and the ensuing SASP. In this study, we engineered and validated a novel lycopene-loaded ceria nanozyme (Ly@Ce) that addressed this multifaceted challenge through the multi-enzyme-like antioxidant activity that broke the cycle of ROS

generation, while the conjugated lycopene not only offered complementary radical quenching but may also facilitate membrane integration and stability.

Our central finding was that the Ly@Ce promoted a profound recovery of mitochondrial function in senescent chondrocytes. The observed reduction in mitochondrial ROS, mitigation of excessive mitochondrial fragmentation, and restoration of mitochondrial membrane potential collectively signified a rescue from the hallmark mitochondrial dysfunction induced by oxidative stress. Crucially, we found that the potent ROS scavenging capacity of nanozymes could also effectively activate NAD^+ production within senescent chondrocytes and alleviated chondrocyte senescence. This positioned Ly@Ce not merely as a passive scavenger, but as an active metabolic modulator. NAD^+ is a linchpin cofactor for sirtuin (Sirt) family deacylases, which are critical guardians of mitochondrial health, biogenesis, and autophagy. By boosting the NAD^+ pool, Ly@Ce significantly enhanced oxidative phosphorylation, promoting mitochondrial quality control *via* fission/fusion balance, and creating a positive feedback loop that reinforced cellular redox homeostasis. This metabolic reprogramming action fundamentally differentiates our approach from conventional antioxidants and underscores the advantage of a nanozyme capable of enzyme-mimetic catalysis within a biological context.

Mechanistically, transcriptomic analysis provided a systems-level insight, revealing that Ly@Ce significantly reversed H_2O_2-induced alterations in the p53-p21 signaling pathway. The p53-p21 axis is a canonical regulator of stress-induced senescence, where persistent DNA damage and mitochondrial distress converge to trigger irreversible cell cycle arrest and SASP. Heatmap analysis of the transcriptome revealed that Ly@Ce nanozyme intervention significantly

reversed the expression of genes regulating the p53-p21 axis and altered cell cycle-related proteins. Concurrently, it decreased the expression of SASP-related genes while increasing the expression of genes involved in anabolic metabolism of cartilage extracellular matrix. Furthermore, it reduced the expression of genes associated with catabolic metabolism. Moreover, Ly@Ce treatment upregulated SIRT1 expression and robustly suppressed the expression of key senescence effectors, p-p53 and p21, and reduced SASP (e.g., IL6, IL13 and IGFBP5) expression. Our results strongly suggested that by rectifying the primary mitochondrial insult and associated metabolic deficit, Ly@Ce alleviated the upstream signals that activated p53, thereby interrupting the core senescence program. This decoupled oxidative stress from its downstream phenotypic consequences, effectively halting the progression from cellular damage to a pro-degenerative senescent state.

Several limitations should be considered when interpreting our results. The mechanism by which Ly@Ce increases NAD^+ levels, whether via upregulation of NAMPT or inhibition of NAD^+ consumers like PARP and CD38-requires further elucidation. Additionally, our conclusions are currently derived from a single H_2O_2-induced oxidative stress model; future studies using diverse senescence models are needed to confirm the generalizability of our findings.

In conclusion, this work presented a bioinspired catalytic nanoplatform that went beyond symptomatic ROS scavenging to actively reprogram the metabolism of senescent chondrocytes. By identifying the p53-p21 axis as a critical therapeutic node and demonstrating its accessibility *via* nanocatalytic medicine, we bridged the gap between mitochondrial bioenergetics and

epigenetically driven senescence in OA. While further investigations are needed to delineate the precise molecular interactions, our findings establish a new paradigm. They highlight the potential of metabolic nanozymes designed to restore crucial metabolic cofactors as a powerful strategy for treating not only OA but also a broad spectrum of age-related diseases characterized by mitochondrial decline and cellular senescence.

1.5 Acknowledgments

This work was supported by the National Natural Science Foundation of China (92368201, 82402863, 82530081, 32301114, W2512074, 22374071), the Natural Science Foundation of Jiangsu Province (BK20232023), the Key Program of Nanozyme Laboratory in Zhongyuan (NLZ-KP2024NIC06), the Jiangsu Provincial Key R&D Program (BE2022836), the State Key Laboratory of Analytical Chemistry for Life Science (5431ZZXM2501), Fundamental Research Funds for the Central Universities (2025300292), the Open Funds of NMPA Key Laboratory for Biomedical Optics (20240001), PAPD Program, the International Expansion and Enhancement Program by Nanjing University International Affairs Office, Yachen Foundation of Nanjing University. Nanjing Municipal Science and Technology Bureau (202305001, 202205020).

1.6 Author contributions

Xueying An: Investigation, Methodology, Formal analysis, Visualization, Funding acquisition, Writing-original draft;

Hanjie Zhang: Investigation, Methodology, Formal analysis, Visualization, Writing-original draft;

Xujing Zhang: Data curation, Validation, Software, Methodology, Visualization;

Minyi Cai: Data curation, Validation;

Yining Zhou: Formal analysis, Software;

Hantao Cai: Validation, Investigation;

Tao Shen: Software, Visualization;

Sheng Zhao: Funding acquisition, Visualization;

Zhihong Xu: Conceptualization, Project administration, Resources, Supervision, Writing-review & editing;

Hui Wei: Conceptualization, Funding acquisition, Resources, Supervision, Writing-review & editing;

Qing Jiang: Conceptualization, Funding acquisition, Project administration, Resources, Supervision, Writing-review & editing.

1.7 Declaration of interest statement

All authors declare that there are no competing interests.

1.8 Availability Statement

The data that support the findings of this study are available from the corresponding author upon reasonable request.

1.9 References

1. Steinmetz JD, Culbreth GT, Haile LM, et al. Global, regional, and national burden of osteoarthritis, 1990–2020 and projections to 2050: a systematic analysis for the Global Burden of Disease Study 2021. The Lancet Rheumatology 2023;5(9):e508-e22. doi: https://doi.org/10.1016/S2665-9913(23)00163-7

2. Hunter DJ, Bierma-Zeinstra S. Osteoarthritis. The Lancet 2019;393(10182):1745-59. doi: https://doi.org/10.1016/S0140-6736(19)30417-9

3. Hunter DJ, March L, Chew M. Osteoarthritis in 2020 and beyond: a Lancet Commission. The Lancet 2020;396(10264):1711-12. doi: https://doi.org/10.1016/S0140-6736(20)32230-3

4. Han Z, Wang K, Ding S, et al. Cross-talk of inflammation and cellular senescence: a new insight into the occurrence and progression of osteoarthritis. Bone Research 2024;12(1):69. doi: 10.1038/s41413-024-00375-z

5. Liu W, Guo N-Y, Wang J-Q, et al. Osteoarthritis: mechanisms and therapeutic advances. MedComm 2025;6(8):e70290. doi: https://doi.org/10.1002/mco2.70290

6. Tang Q, Zheng G, Feng Z, et al. Trehalose ameliorates oxidative stress-mediated mitochondrial dysfunction and ER stress via selective autophagy stimulation and autophagic flux restoration in osteoarthritis development. Cell Death & Disease 2017;8(10):e3081-e81. doi: 10.1038/cddis.2017.453

7. Coryell PR, Diekman BO, Loeser RF. Mechanisms and therapeutic implications of cellular senescence in osteoarthritis. Nature Reviews Rheumatology 2021;17(1):47-57. doi: 10.1038/s41584-020-00533-7

8. Johansen M, Bahrt H, Altman RD, et al. Exploring reasons for the observed inconsistent trial reports on intra-articular injections with hyaluronic acid in the treatment of osteoarthritis: Meta-regression analyses of randomized trials. Seminars in Arthritis and Rheumatism 2016;46(1):34-48. doi: https://doi.org/10.1016/j.semarthrit.2016.02.010

9. van Middelkoop M, Arden NK, Atchia I, et al. The OA Trial Bank: meta-analysis of individual

patient data from knee and hip osteoarthritis trials show that patients with severe pain exhibit greater benefit from intra-articular glucocorticoids. Osteoarthritis and Cartilage 2016;24(7):1143-52. doi: https://doi.org/10.1016/j.joca.2016.01.983

10. Bannuru RR, Osani MC, Vaysbrot EE, et al. OARSI guidelines for the non-surgical management of knee, hip, and polyarticular osteoarthritis. Osteoarthritis and Cartilage 2019;27(11):1578-89. doi: https://doi.org/10.1016/j.joca.2019.06.011

11. da Costa BR, Reichenbach S, Keller N, et al. Effectiveness of non-steroidal anti-inflammatory drugs for the treatment of pain in knee and hip osteoarthritis: a network meta-analysis. The Lancet 2017;390(10090):e21-e33. doi: https://doi.org/10.1016/S0140-6736(17)31744-0

12. Lützner J, Kasten P, Günther K-P, et al. Surgical options for patients with osteoarthritis of the knee. Nature Reviews Rheumatology 2009;5(6):309-16. doi: 10.1038/nrrheum.2009.88

13. Li Y, He X, Yin J-J, et al. Acquired superoxide-scavenging ability of ceria nanoparticles. Angewandte Chemie International Edition 2015;54(6):1832-35. doi: https://doi.org/10.1002/anie.201410398

14. Korsvik C, Patil S, Seal S, et al. Superoxide dismutase mimetic properties exhibited by vacancy engineered ceria nanoparticles. Chemical Communications 2007(10):1056-58. doi: 10.1039/B615134E

15. Zhao S, Li Y, Liu Q, et al. An orally administered CeO2@montmorillonite nanozyme targets Inflammation for inflammatory bowel disease therapy. Advanced Functional Materials 2020;30(45):2004692. doi: https://doi.org/10.1002/adfm.202004692

16. Chen H, Ye T, Hu F, et al. Urchin-like ceria nanoparticles for enhanced gene therapy of osteoarthritis. Science Advances 2023;9(24):eadf0988. doi: doi:10.1126/sciadv.adf0988

17. Dong S, Dong Y, Liu B, et al. Guiding transition metal-doped hollow cerium tandem nanozymes with elaborately regulated multi-enzymatic activities for intensive chemodynamic therapy. Advanced Materials 2022;34(7):2107054. doi: https://doi.org/10.1002/adma.202107054

18. Yao C, Wang W, Wang P, et al. Near-Iinfrared upconversion mesoporous cerium oxide hollow biophotocatalyst for concurrent pH-/H2O2-responsive O2-evolving synergetic cancer therapy. Advanced Materials 2018;30(7):1704833. doi: https://doi.org/10.1002/adma.201704833

19. Wu Z, Zhang X, Li Z, et al. Activation of autophagy contributes to the protective effects of lycopene against oxidative stress-induced apoptosis in rat chondrocytes. Phytotherapy Research 2021;35(7):4032-45. doi: https://doi.org/10.1002/ptr.7127

20. Zhan J, Yan Z, Kong X, et al. Lycopene inhibits IL-1β-induced inflammation in mouse chondrocytes and mediates murine osteoarthritis. Journal of Cellular and Molecular Medicine 2021;25(7):3573-84. doi: https://doi.org/10.1111/jcmm.16443

21. Wu H, Wu Y, Cui Z, et al. Nutraceutical delivery systems to improve the bioaccessibility and bioavailability of lycopene: A review. Critical Reviews in Food Science and Nutrition 2024;64(18):6361-79. doi: 10.1080/10408398.2023.2168249

22. Li Y, Cui Z, Hu L. Recent technological strategies for enhancing the stability of lycopene in processing and production. Food Chemistry 2023;405:134799. doi: https://doi.org/10.1016/j.foodchem.2022.134799

23. Muhammad F, Huang F, Cheng Y, et al. Nanoceria as an Electron Reservoir: Spontaneous

Deposition of Metal Nanoparticles on Oxides and Their Anti-inflammatory Activities. ACS Nano 2022;16(12):20567-76. doi: 10.1021/acsnano.2c07306

24. Lin A, Liu Q, Zhang Y, et al. A Dopamine-Enabled Universal Assay for Catalase and Catalase-Like Nanozymes. Analytical Chemistry 2022;94(30):10636-42. doi: 10.1021/acs.analchem.2c00804

25. Gomes Ana P, Price Nathan L, Ling Alvin JY, et al. Declining NAD+ induces a pseudohypoxic state disrupting nuclear-mitochondrial communication during aging. Cell 2013;155(7):1624-38. doi: https://doi.org/10.1016/j.cell.2013.11.037

26. Wang B, Wang L, Gasek NS, et al. Intermittent clearance of p21-highly-expressing cells extends lifespan and confers sustained benefits to health and physical function. Cell Metabolism 2024;36(8):1795-805.e6. doi: https://doi.org/10.1016/j.cmet.2024.07.006

27. Martel-Pelletier J, Barr AJ, Cicuttini FM, et al. Osteoarthritis. Nature Reviews Disease Primers 2016;2(1):16072. doi: 10.1038/nrdp.2016.72

28. Tang Sa, Zhang C, Oo WM, et al. Osteoarthritis. Nature Reviews Disease Primers 2025;11(1):10. doi: 10.1038/s41572-025-00594-6

29. Motonari H, Hayashi A, Tanaka Y, et al. Mitochondrial dysfunction exacerbates inflammatory responses via the JNK/p38-AP-1 pathway in primary cultured chondrocytes. International Immunopharmacology 2025;165:115433. doi: https://doi.org/10.1016/j.intimp.2025.115433

30. He S, Sharpless NE. Senescence in Health and Disease. Cell 2017;169(6):1000-11. doi: https://doi.org/10.1016/j.cell.2017.05.015

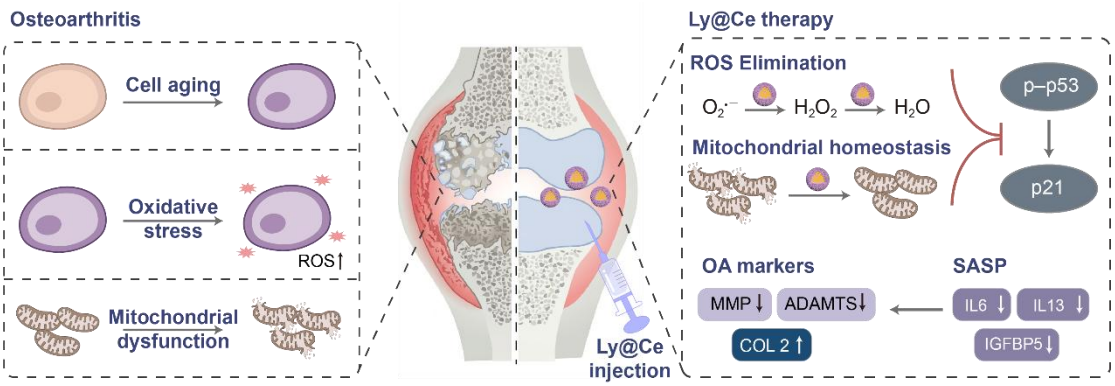

Scheme 1. Schematic illustration of Ly@Ce-mediated protection against OA. By reducing ROS levels and alleviating mitochondrial damage in chondrocytes, Ly@Ce blocks the p53-p21 axis, inhibits the secretion of SASP factors, and restores extracellular matrix homeostasis, there by delaying OA progression.

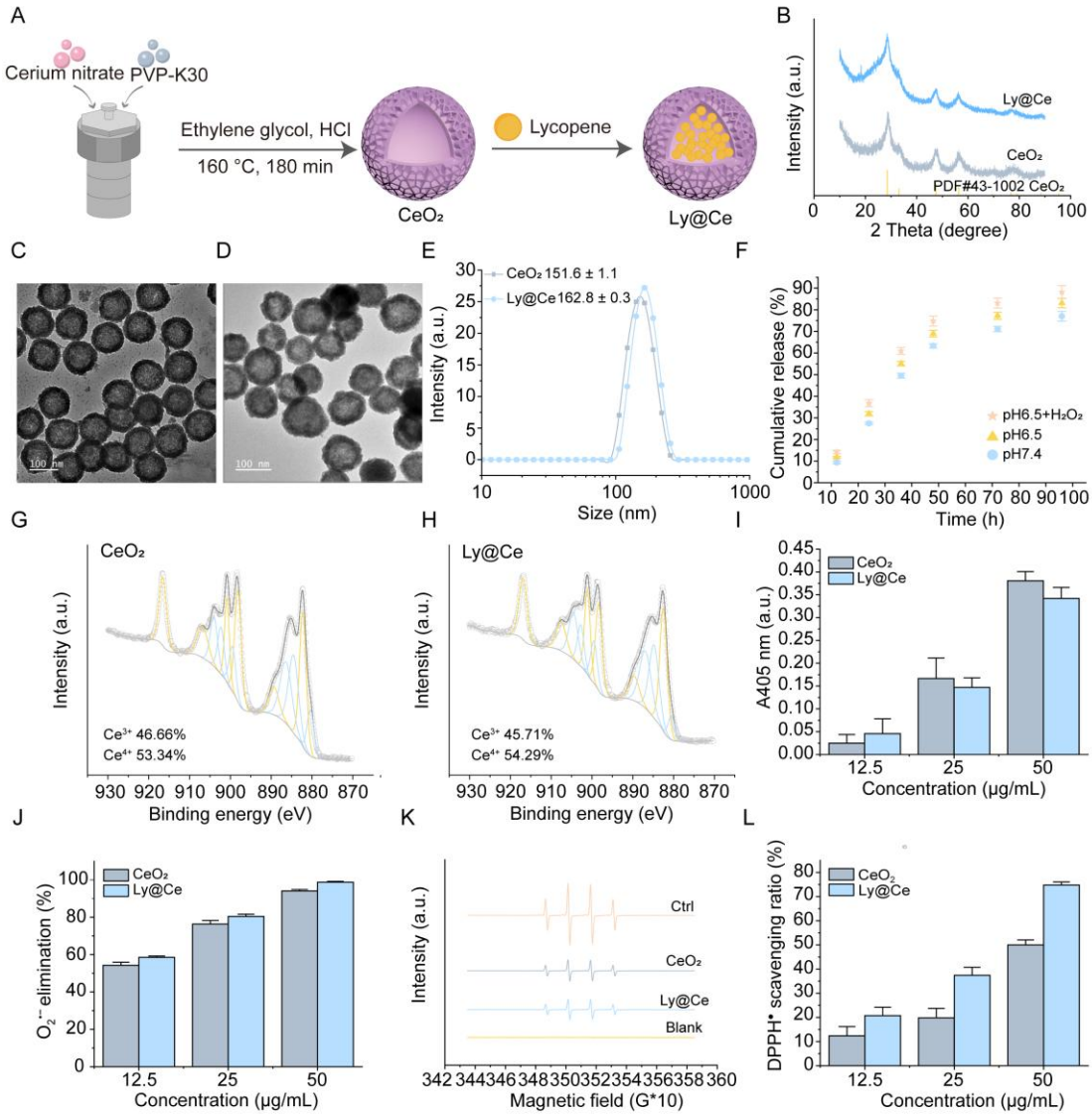

Figure 1. Synthesis, characterization, and enzyme-like activity assays of Ly@Ce. (A) Schematic diagram of Ly@Ce synthesis. (B) XRD patterns of CeO_2 and Ly@Ce. the yellow lines at the bottom mark the reference patterns of CeO_2 (PDF#43-1002) from JCPDS database. TEM images of (C) CeO_2 and (D) Ly@Ce. (E) DLS analysis of CeO_2 and Ly@Ce. (F) Cumulative release of lycopene from the hollow CeO_2 drug delivery system. Ce 3*d* XPS spectra of (G) CeO_2 and (H) Ly@Ce. (I) CAT- and (J) SOD-like activities of CeO_2 and Ly@Ce. (K) EPR analysis for elimination of $^{\bullet}OH$. (L) $DPPH^{\bullet}$ scavenging ratio of CeO_2 and Ly@Ce. Data were presented as

mean ± SD, n = 3. a.u., arbitrary units.

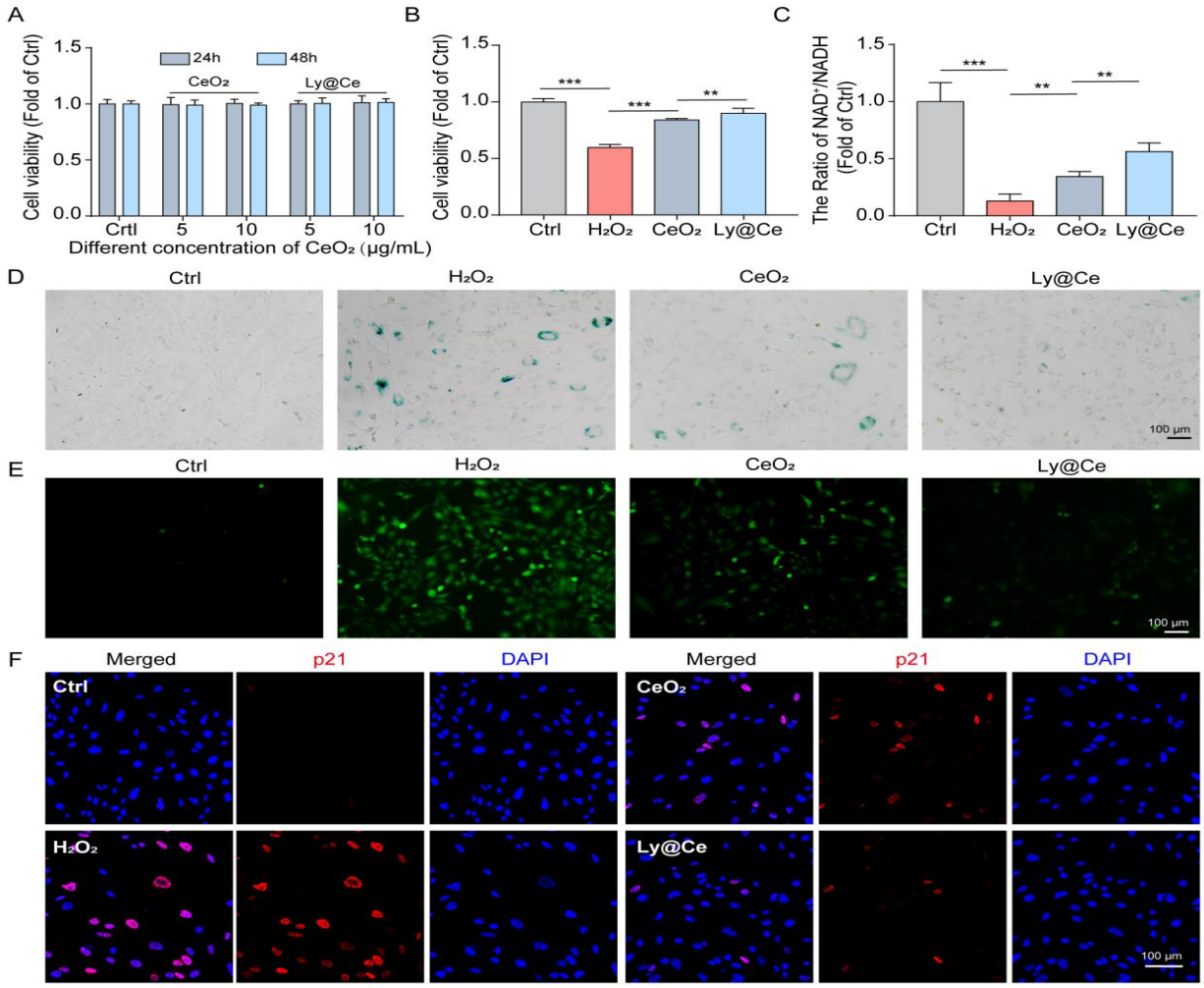

Figure 2. Ly@Ce attenuates chondrocyte senescence and cellular oxidative stress levels. (A) Cell viability after 24 h or 48 h incubation with CeO_2 or Ly@Ce. (B-C) Cell viability and the ratio of NAD^+/NADH in chondrocyte after 24 h incubated with CeO_2 or Ly@Ce under H_2O_2 treatment. (D) Representative microscopic images of chondrocytes stained with SA-β-gal. Representative Fluorescence microscopy images of chondrocytes staining with (E) DCFH-DA and (F) p21. Data in (A, B) was presented as mean ± SD, n = 8. Data in (C) was presented as mean ± SD, n = 4. Statistical differences were analyzed by one-way ANOVA and Student's t-test:

*p<0.05, **p<0.01, and ***p<0.001.

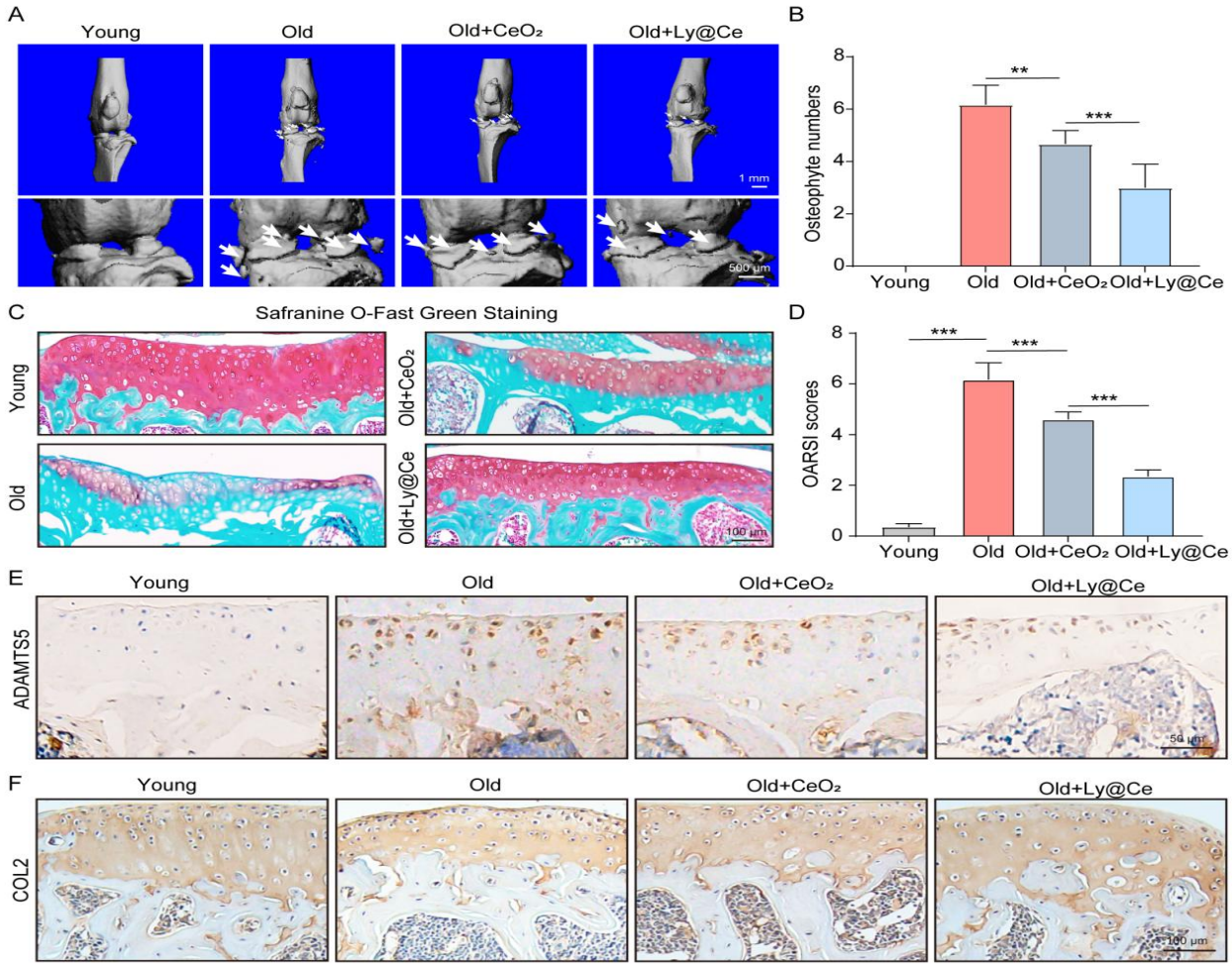

Figure 3. Ly@Ce alleviates OA progression in aged mice. (A) Representative micro-CT images of knee-joint after the indicated treatments. (B) Quantitative assessment of osteophyte number per joint. (C) Representative Safranin O-Fast Green staining images of knee joints. (D) Quantification of OARSI scores Representative immunohistochemical staining images of (E) ADAMTS5 and (F) COL2 in knee articular cartilage. Data was presented in (B) and (D) as mean ± SD, n = 6. Statistical differences were analyzed by one-way ANOVA and Student's t-test: *p<0.05, **p<0.01, and ***p<0.001.

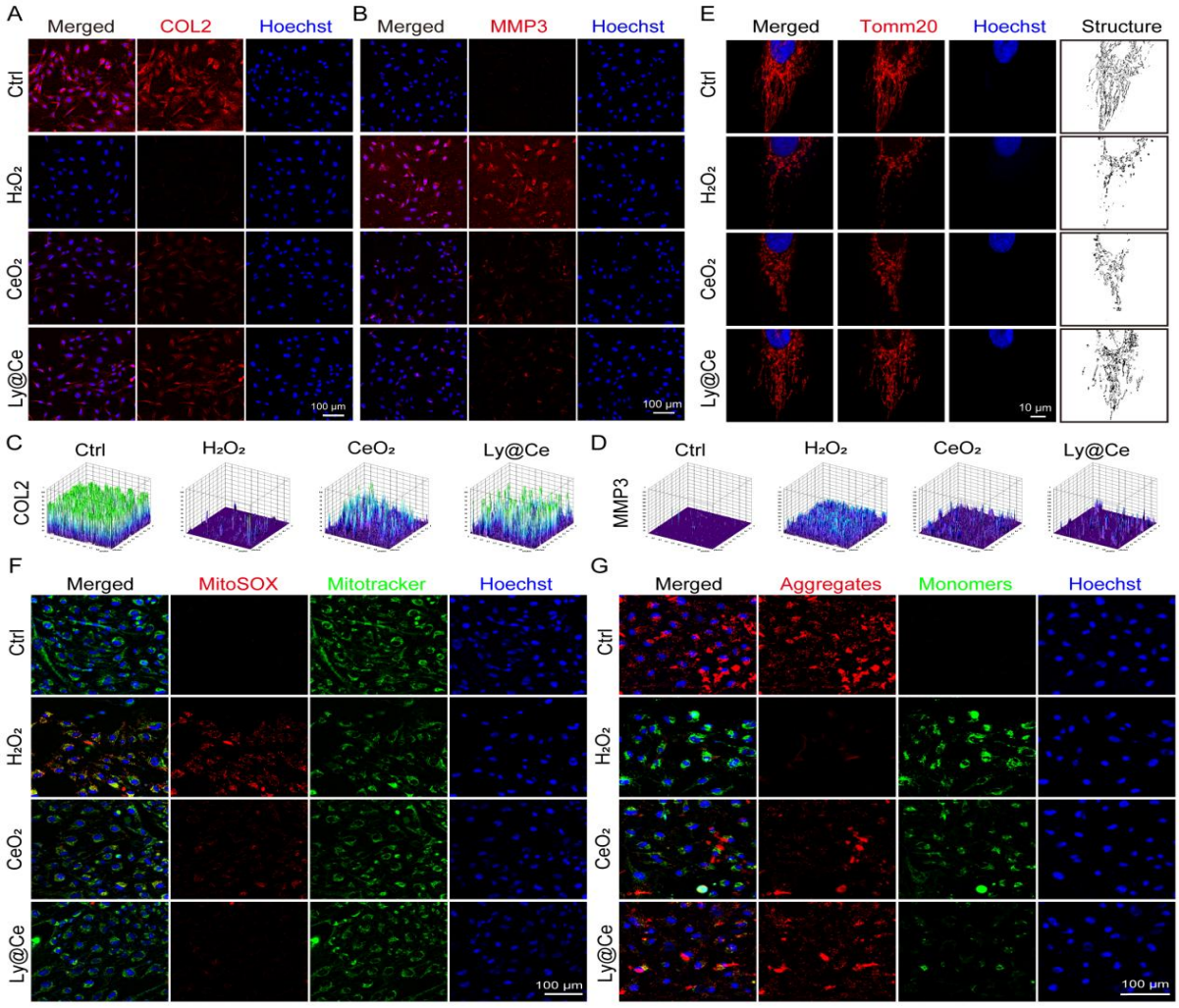

Figure 4. Ly@Ce suppresses OA-like phenotypes and mitochondrial dysfunction in senescent chondrocytes. Immunofluorescence staining of (A) COL2 and (B) MMP3 in chondrocytes after treatment with CeO_2 or Ly@Ce in H_2O_2-induced senescent chondrocytes. Heatmap analysis of IF for COL2 (C) and MMP3 (D) of chondrocytes in different groups after 24 h incubation. (E) Representative immunofluorescence images of mitochondrial morphology in chondrocytes stained for Tomm20 (red) and nuclei (Hoechst, blue). (F) Mitochondrial ROS levels and (G) Mitochondrial membrane potential in chondrocytes after treatment with CeO_2 or Ly@Ce in H_2O_2-induced senescent chondrocytes.

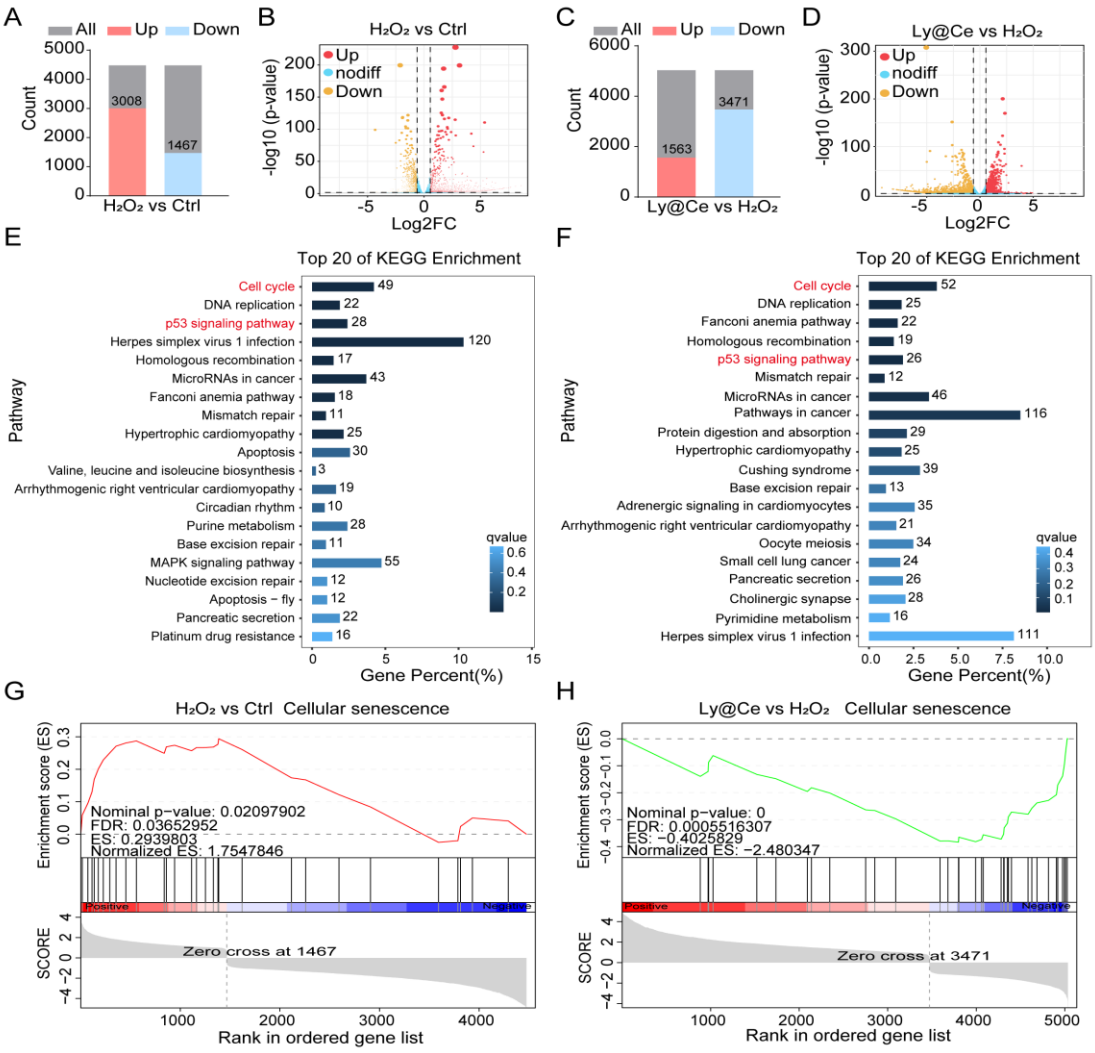

Figure 5. Transcriptome sequencing revealed Ly@Ce nanozyme alleviated chondrocyte senescence. (A, B) Summary of DEGs and volcano plot of chondrocytes after H_2O_2 stimulation. (C, D) Summary of DEGs and volcano plot of H_2O_2 stimulated chondrocytes following treatment with Ly@Ce. (E) KEGG analysis of genes differentially expressed in chondrocytes treated with H_2O_2 compared with the control group. (F) KEGG analysis of genes differentially expressed in chondrocytes treated with Ly@Ce compared with the H_2O_2 group. (G) GSEA analysis of cell senescence by differentially expressed genes across H_2O_2 and control group. (H) GSEA analysis of cell senescence by differentially expressed genes across Ly@Ce and H_2O_2 group.

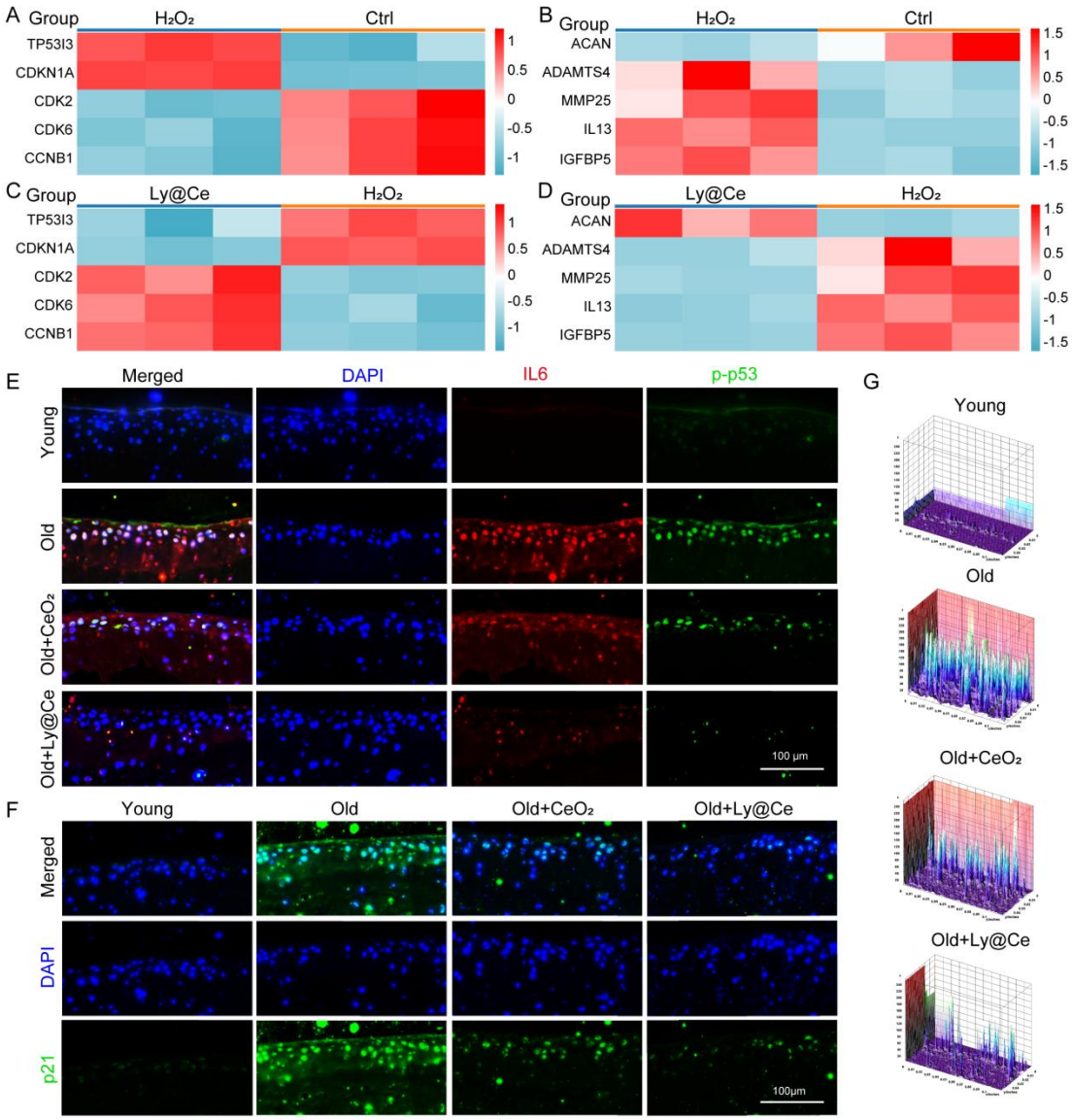

Figure 6. Ly@Ce alleviates chondrocyte senescence by inhibiting the p53-p21 axis. Heatmap analysis of (A) DEGs in the TP53 signaling pathway and (B) OA-related genes and SASP genes in chondrocytes after H_2O_2 stimulation. Heatmap analysis of (C) DEGs in the TP53 signaling pathway and (D) OA-related genes and SASP genes in H_2O_2 stimulated chondrocytes after treatment with Ly@Ce. (E) Immunofluorescence staining of p-p53 and IL6 in knee joint cartilage following Ly@Ce treatment. (F) Immunofluorescence staining and (G) heatmap analysis of p21 expression in knee joint cartilage after Ly@Ce treatment.

Highlights

A lycopene-loaded CeO_2 nanozyme (Ly@Ce) is developed to combat chondrocyte senescence for osteoarthritis therapy

Ly@Ce efficiently scavenges mitochondrial ROS, restores mitochondrial dynamics, and elevates NAD^+ levels

Ly@Ce reverses H_2O_2-induced dysregulation of the p53-p21 signaling axis

Ly@Ce suppresses SASP expression and shifts ECM metabolism toward an anabolic program

The nanozyme integrates redox/NAD^+ reprogramming with senescence pathway inhibition, offering a disease-modifying strategy for OA